Applying Stray Inductance Model to Study Turn-OFF Current in Multi-Turn Loop of Shallow Transient Electromagnetic Systems

Lihua Liu, Liu Qiao, Leisong Liu, Zhi Geng, Zongyang Shi, and Guangyou Fang

***Abstract*—The multi-turn, small loop is usually used as the transmitting loop for shallow transient electromagnetic (TEM) surveying. As an inductive load of the current inverter of the TEM system, it finds that there are serious oscillations at early part of the turn-off current. However, the existed *RLC* equivalent model of the loop alone fails to explain this phenomenon. In this paper, a novel current inverter for shallow TEM survey is designed and analyzed. The passive constant voltage clamping technology is used to achieve fast linear turn-off current. Furthermore, a novel stray inductance model of the current inverter is first proposed and utilized to analyze the serious oscillations of turn-off current. Based on this model, the turn-off current of the current inverter is simulated, and the simulated results agree well with the measured results of the experiment, which verifies that the proposed stray inductive model is effective and reasonable. According to the TEM principle, the high-frequency oscillations of the early part turn-off current will badly influence the shallow transient electromagnetic response. In order to suppress the oscillations of the turn-off current, two effective suppressing methods are proposed and analyzed. It will effectively enhance the electromagnetic data interpretation quality for shallow TEM survey.**

***Index Terms*—Current inverter, current oscillations, multi-turn loop, stray inductance, transient electromagnetic system, turn-off current.**

I. Introduction

THE multi-turn loop is widely used as an inductive load of the current transmitter for the transient electromagnetic (TEM) surveying [1], [2]. The geometry size of the square loop is usually from approximately 1 m × 1 m up to 1000 m × 1000 m or even larger, and laid out on the earth surface for ground survey or towed by the aircraft for aero-borne survey. For the ground shallow TEM survey, the geometry size of the transmitting loop is smaller than the deep survey, usually from 1 m × 1 m to 10 m ×10 m with multi turns, such as 10 to 200 turns.

Manuscript received February 18, 2019; revised April 20, 2019; accepted May 31, 2019. Date of publication June 16, 2019; date of current version November 12, 2019. This work was supported in part by the National Key Research and Development Program Major Scientific Instruments and in part by the Equipment Development Key Projects of China under Grant 2018YFF01013300. Recommended for publication by Associate Editor F. Costa. *(Corresponding author: Lihua Liu.)*

The authors are with the Key Laboratory of Electromagnetic Radiation and Sensing Technology, Institute of Electronics, Chinese Academy of Sciences, Beijing 100190, China (e-mail: lhliu@mail.ie.ac.cn; qiaoliu@126.com; lsliu@mail.ie.ac.cn; gengzhi@126.com; zongyangshi13@163.com; gyfang@mail.ie.ac.cn).

Color versions of one or more of the figures in this paper are available online at http://ieeexplore.ieee.org.

Digital Object Identifier 10.1109/TPEL.2019.2923234

Current inverter [3]–[6] is one of the most important components of the TEM systems. The typical pulse shape of the current inverter is the bipolar square pulses, which have a peak current of several to several tens Amperes are injected into the transmitting loop. The eddy currents in the subsurface of the earth are induced during the turn-off step and propagate downward and outward gradually. A receiver, located at some offset to the transmitting loop, records the electromagnetic responses of the secondary field in the forms of the time derivative of the magnetic field and the electric field components. The electromagnetic response data are typically used for modeling and inversions to interpret and identify the underground anomalies of interest.

Generally, the key parameters of the square current pulse include the pulse amplitude, pulse duration, pulse repetition frequency, and the turn-off time of the current's falling edge. For the TEM system, the current's turn-off characteristic [7]–[9] is one of the most important factors for the transient electromagnetic responses and data interpretation [10]–[12]. During the current's turn-off stage, the primary transient responses and the secondary transient responses carrying the early time information of the underground targets both exist. Therefore, it is important to improve the quality of the turn-off current for better acquisition of early electromagnetic response and enhancing the shallow survey ability.

Usually, the multi-turn loop can be equivalent to a *RLC* lumped circuit model. The *R*, *L*, *C* are the equivalent resistance, inductance, and capacitance of the transmitting loop, respectively. Compared to the single turn loop, the multi-turn loop has larger inductance and non-negligible capacitance for the turn-to-turn gap of the loop. It means that it is impossible to achieve an ideal step current in the loop due to its load characteristics. In fact, the actual turn-off process of the current needs to take some time, such as tens to hundreds of microseconds to turn off thoroughly.

Generally, the turn-off current could be divided into three parts, the early part, the medium part, and the later part. For the medium part, it is usually optimized by the technique of constant voltage clamping to realize linear and fast decay. For the later part, the current overshoots, which are usually inevitable, have some bad effects on the transient response for data processing and target detection, are suppressed and optimized by utilizing the damping circuit [13]. However, for the early part, there are serious high-frequency oscillations in multi-turn loop, which could not be explained reasonably until now. Therefore, it is

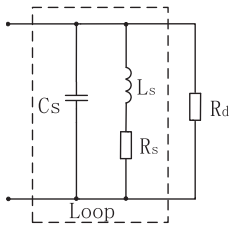

Fig. 1. Equivalent lumped parameter circuit of the multi-turn loop.

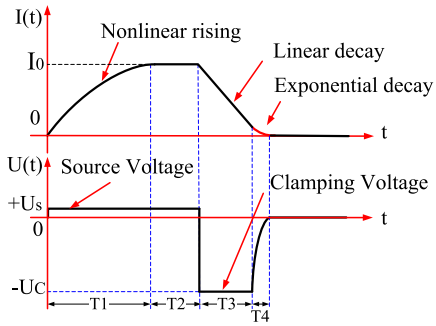

Fig. 2. Current and voltage waveform of the loop under clamping.

very difficult to design the current inverter for the multi-turn loop and suppress the oscillations of the turn-off current.

The usual methods to suppress the current overshoots or oscillations mainly include three kinds of snubber circuit [14]–[16], such as the resistor-capacitance-diode (RCD), resistor-capacitance (RC), and C network, which are parallel to the insulated gate bipolar transistors (IGBTs) of the current inverter. They can suppress the inrush voltage when the IGBTs shut off thus protect the IGBTs from damage. However, when the load of the current converter is the multi-turn loop of the shallow TEM system, the above three snubber circuits could not suppress the oscillations effectively.

In this paper, a novel current inverter is designed and developed for shallow TEM survey. A novel stray inductance model of the current inverter is first established and applied to analyze the existed serious oscillations of the turn-off current. Based on the stray inductance model of the current inverter circuit, combined with the equivalent *RLC* lumped model of the multi-turn loop, the turn-off current simulated by the MATLAB Simulink agrees very well with the measured results of the inverter prototype. It verifies that the stray inductance model is effective to explain the existed serious oscillations. Furthermore, the suppressing methods in order to decrease the turn-off current oscillations are also proposed and analyzed. The current oscillations are suppressed effectively to enhance the quality of the early turn-off current for the shallow TEM survey.

II. Design of Current Inverter

A. Analysis of the Multi-Turn Loop

The multi-turn transmitting loop is usually regarded as an inductive load, just like a large inductor, and the basic equivalent lumped parameter circuit of the loop is shown in the dashed part of Fig. 1. L_s is the total inductance and it includes main and leakage inductances, R_s is the serial connection of ac winding resistance, C_s represents the stray capacitance [17]. Inductance and resistance are frequency dependent, due to the skin and proximity effect in the winding. Stray capacitance is assumed to be frequency independent. R_d is the damping resistor which is parallel to the loop shown in Fig. 1. It is utilized to suppress the current overshoot and damp the ringing for the transient applications.

Circuit analysis can be used to obtain an expression for the input impedance associated with the equivalent circuit in Fig. 1. By summing the admittances for the three parallel branches, the input impedance is

$$Z_i = R_i + jX_i = \left[\frac{1}{R_s + j\omega L_s} + j\omega C_S + \frac{1}{R_d}\right]^{-1}. \quad (1)$$

Then, the input resistance and input reactance can be obtained

$$R_i = \frac{R_s\left[1 + \frac{R_s}{R_d} + \frac{(\omega L_s)^2}{R_s R_d}\right]}{\left(1 + \frac{R_s}{R_d} - \omega^2 L_s C_s\right)^2 + \left(\frac{\omega L_s}{R_d} + \omega C_s R_s\right)^2}$$
$$X_i = \frac{\omega L_s(1 - \omega^2 L_s C_s) - {R_s}^2 \omega C_s}{\left(1 + \frac{R_s}{R_s} - \omega^2 L_s C_s\right)^2 + \left(\frac{\omega L_s}{R_s} + \omega C_s R_s\right)^2}. \quad (2)$$

The series resonant frequency can be calculated when $X_i = 0$

$$f_{\text{SRF}} = \frac{1}{2\pi}\sqrt{\frac{L_s - R_s^2 C_s}{L_s^2 C_s}}. \quad (3)$$

It can be simplified as follows:

$$f_{\text{SRF}} = \frac{1}{2\pi\sqrt{L_s C_s}} \text{ if } R_S \ll \sqrt{\frac{L_s}{C_s}} = \omega_{\text{SRF}} L_S. \quad (4)$$

Generally, its stray capacitance C_s of multi-turn transmitting loop is several to tens pF, which is much smaller compared to the total inductance L_s so that it is usually not considered for analysis under the effect of the constant clamping technique ideally. The corresponding ideal current waveform of the loop for the TEM applications, taking the positive pulse, for example, is shown in Fig. 2. The positive current pulse rises according to the rule of the exponential function during the time T1, and goes into a stable amplitude powered by the dc source U_s during the time T2. Then, the current turns off in linear decay during the time T3 under the action of clamping circuit. The corresponding turn-off voltage is clamped to a constant high amplitude, such as 500–1000 V under the constant clamping technique [18]. The short tail of the turn-off current during the T4 is an exponential decay by the work of the damping circuit. Therefore, the corresponding mathematical expression of the current during different periods

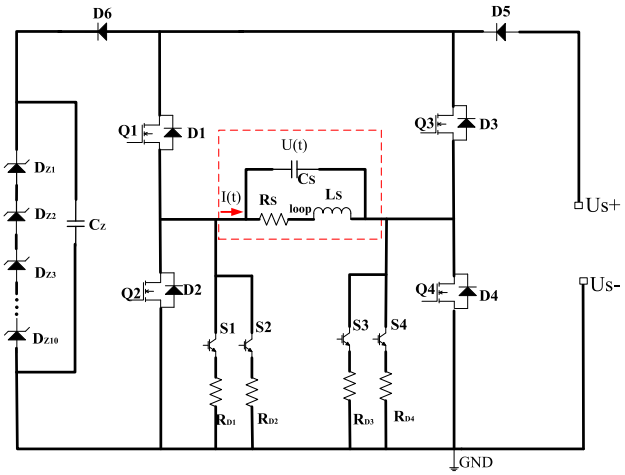

Fig. 3. Diagram of current inverter with damping resistors.

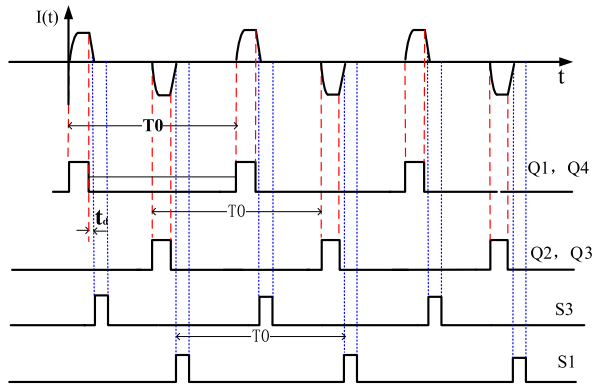

Fig. 4. Control signals of the current inverter.

according to Fig. 2 is as follows:

$$\begin{cases} I(t) = \frac{U_s}{R_s}\left(1 - e^{-\frac{R_S}{L_S}t}\right) = I_0\left(1 - e^{-\frac{R_S}{L_S}t}\right) & t \in T1 \\ I(t) = \frac{U_s}{R_s} = I_0 & t \in T2 \\ I(t) = -\frac{U_C}{L_S}(t - T1 - T2) + I_0 & t \in T3 \\ I(t) = -\frac{U_C}{R_S}\left(1 - e^{-\frac{R_D}{L_S}(t - T1 - T2 - T3)}\right) & t \in T4. \end{cases} \tag{5}$$

However, in practical circuit design, especially for the multi-turn loop, whose stray capacitance C_s is usually several nF so that it is not negligible, it will generate some high-frequency signals added to the turn-off current. This problem will be analyzed and resolved in the next parts.

B. Design of the Current Inverter

Based on the above analysis of the multi-turn loop, a novel bipolar square current inverter for the shallow TEM survey is designed. The turn-off process of the current is controlled by using the passive constant voltage clamping technology and thus to realize fast and linear falling edge with a turn-off time of several tens of milliseconds. Fig. 3 is the designed current inverter circuit, which converts the dc source U_s to bipolar square current pulse. The Q1, Q2, Q3, and Q4 are high-power and high-speed MOSFET modules, with inner diodes D1, D2, D3, and D4. The D5 is an isolated diode between the dc source and the bridge circuit. There are four isolated triggering circuits for driving the Q1, Q2, Q3, and Q4 of the inverter. D_{Z1} to D_{Z10} are Zener diodes for passive clamping the voltage during the current's turn-off time. The capacitor C_Z is parallel to the Zener diodes to ensure much more stable clamping voltage.

The principle of the passive constant voltage clamping is that the Zener diodes are used to absorb the discharge energy of the multi-turn loop when the current inverter is switched off. Generally, for the high-power current inverter, the discharge energy is stored in a capacitor bank and recycled in the next period. For the shallow TEM applications, it requires the current inverter has a much faster turn-off speed to obtain high-frequency electromagnetic responses. It is not necessary for the current amplitude to be very large for shallow survey, so a stable and compact design of the current inverter choose the Zener diodes bank for fast decay of the current's falling edge.

Usually, the current overshoot will appear and last a few milliseconds for the parasitical parameters of the loop. An overshoot inhibition circuit or named damping circuit, which is composed of damping resistor R_{D1}, R_{D2}, R_{D3}, R_{D4} and S1, S2, S3, S4, is used to suppress the current overshoot. There are three to seven provided damping resistor pairs for the positive pulse and negative pulse, respectively. For practical applications, the appropriate damping resistor pair should be selected according to the loop parameters to suppress the current overshoot effectively.

The control signals for the switches generated by the current inverter's control unit based on the FPGA are shown in Fig. 4. The first two logical signals are used to drive the Q1, Q4 of the positive half-bridge circuit and Q2, Q3 of the negative half-bridge circuit, respectively. Another two logical signals are used to drive the S1 and S3 of the overshoot inhibition circuit to suppress the overshoot of the current's falling edge. T_0 is the base frequency of the current inverter, and t_d is the delay time between the S3 switches ON and the Q1, Q4 switch off just before the current drops to zero. The value of t_d is in a range from several microseconds to several hundred microseconds according to the current's turn-off time.

The following analysis of the current inverter circuit is under the condition that the damping resistor pair R_{D1} and R_{D3} are chosen for suppressing the current overshoot.

Fig. 5(a) shows the first half cycle of positive current pulse generating circuit in the stage of T1 and T2. Q1 and Q4 are triggered ON, and the inverter is powered by the dc source U_s. The current of the multi-turn loop is i_L and its direction is shown as the red line. Fig. 5(b) shows the circuit when the current turns off in the stage of T3. The clamping circuit composed of D_{Z1} to D_{Z10} and C_Z begins to work, and the C_s of the loop is not negligible for the turn-off current. In the stage of T3, the Zener diodes are reverse turned ON when the induced voltage of the loop is higher than the total Zener voltage. During this time, the power stored in the inductive loop is consumed by the Zener diodes, and the falling current turns off linearly and quickly in

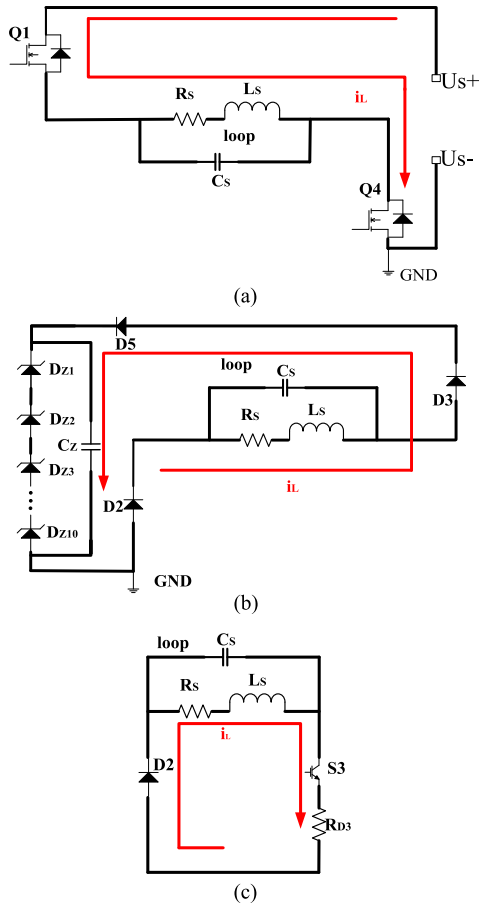

Fig. 5. Positive half circle operating model. (a) Circuit of positive current pulse in the stage of T1 and T2. (b) Circuit of positive current pulse in the stage of T3. (c) Circuit of overshoot inhibition in the stage of T4.

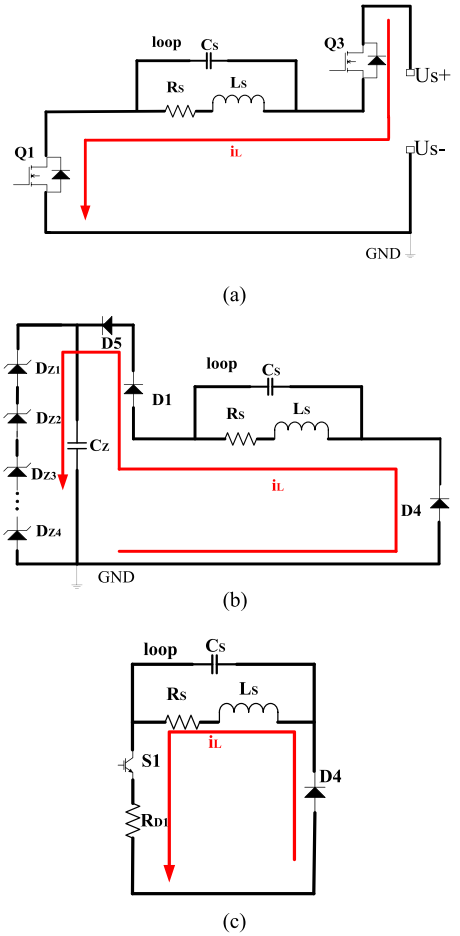

Fig. 6. Negative half circle operating model. (a) Circuit of negative current pulse in the stage of T1 and T2. (b) Circuit of negative current pulse in the stage of T3. (c) Circuit of overshoot inhibition in the stage of T4.

a short time. Usually, the clamping voltage sets as 500–1000 V for the TEM design.

Fig. 5(c) shows the damping circuit in the stage of T4. Ideally, the damping circuit begins to work when the current drops to zero. However, it is hard to accurately determine the time of zero current, so the overshoot inhibition circuit begins to work at a short time such as several microseconds before the current drops to zero for applications. S3, L_S, R_S, C_s, inner diode D2 of Q2, and damping resistor R_{D3} in series constitute a discharge path to suppress the positive current overshoot. The overshoot inhibition circuit will continue to work for a short time until the current overshoot decreases to zero completely. During the short time of T4, the current decays as exponential rule.

Similarly, in the second half cycle of negative current pulse shown in Fig. 6(a), Q2 and Q3 are triggered on and the inverter is powered by the dc source U_s. During this process, the amplitude of the negative pulse rises as the exponential rule and then goes into a stable value. Fig. 6(b) shows the circuit of the turning off process under the work of the clamping circuit. During this process of the negative pulse, the turn-off current decays as linear rule. Fig. 6(c) shows the damping circuit for the negative pulse. Same to the positive cycle, the S1, L_S, R_S, C_s, the inner diode D4 of Q4, and damping resistor R_{D1} in series constitute a discharge path to suppress the negative current overshoot. By the work of the overshoot inhibition circuit, the tail of the falling current that decays to zero follows the exponential rule.

III. Simulation of Current Inverter Based on Stray Inductance Model

A. Analysis of Stray Inductance Model of Current Inverter

Mostly, the TEM systems pay less attention to the effects of the stray inductances [19]–[27] of the current inverter itself. Generally, for the single or several turns transmitting loop, the stray inductance of the inverter has not much influence to the turn-off current thus it usually could be ignored. However, for the multi-turn loop, the stray inductance of the current inverter could not be ignored as before, and has to be considered together with the equivalent lumped parameters of the multi-turn loop to analyze the turn-off current of the inverter.

The stray inductance of the current inverter mainly includes three aspects [28]–[33]: the bus bar inductance, the bus bar to power device or power module stray inductance, and the inner stray inductance of the MOSFET module. Fig. 7 illustrates the equivalent circuit of the current inverter based on the stray inductance model. L_1 to L_{10} are the bus bar stray inductance. L_{11}, L_{13}, L_{15}, and L_{17} are the stray inductances of bus bar to collector of the MOSFETs. L_{12}, L_{14}, L_{16}, and L_{18} are the stray

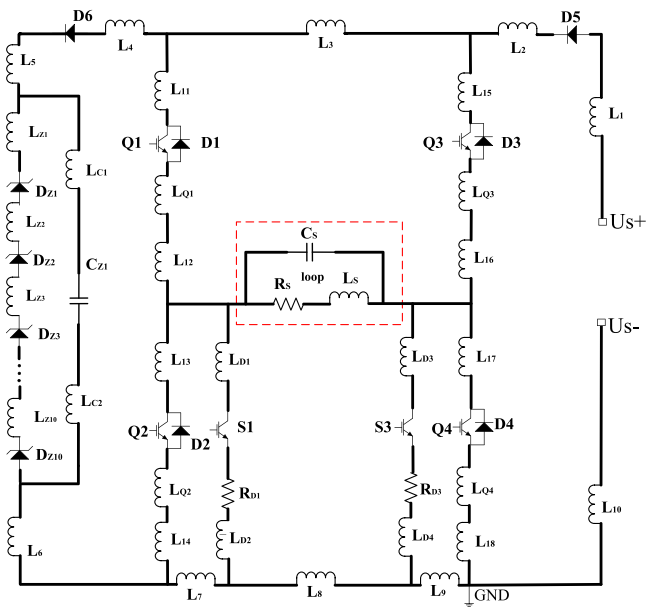

Fig. 7. Current inverter circuit based on the stray inductance model.

TABLE I
SIMULATED STRAY INDUCTANCE OF CURRENT INVERTER

Parameters	Value
L_1,L_2,L_3,L_4,L_5,L_6, L_7,L_8 L_9,L_{10}	60 nH
L_{11}, L_{13}, L_{15}, L_{17}	86 nH
L_{12}, L_{14}, L_{16}, L_{18}	40 nH
L_{Q1},L_{Q2},L_{Q3},L_{Q4}	42 nH
L_{C1},L_{C2}	30 nH
L_{D1}, L_{D2}, L_{D3}, L_{D4}	70 nH
L_{Z1},L_{Z2},L_{Z3},L_{Z4},L_{Z5},L_{Z6},L_{Z7},L_{Z8},L_{Z9},L_{Z10}	84 nH
	75 nH

inductances of the bus bar to the emitter of the MOSFETs. L_{Q1}, L_{Q2}, L_{Q3}, and L_{Q4} are the inner stray inductances of Q1, Q2, Q3, and Q4, respectively [33]–[35]. L_{C1} and L_{C2} are the stray inductances of bus bar to the capacitor of clamping circuit. L_{Z1} to L_{Z10} are the total stray inductance of bus bar to the Zener diodes. The L_{D1}, L_{D2}, L_{D3}, and L_{D4} are the stray inductances of bus bar to the damping circuit.

The stray inductances of the inverter circuit are mainly from the printed line on the PCB board, and could be calculated using the following formula:

$$L = \frac{\mu_0 l}{2\pi}\left(\ln\frac{2l}{w} + 0.5 + 0.2235\frac{w}{l}\right) \tag{6}$$

where l is the length of the wire, w is the width of strip line, and $\mu_0 = 4\pi \times 10^{-7}\mathrm{H/m}$.

According to the above formula (6), the values of the stray inductances of Fig. 6 and the equivalent lumped parameters of the loop are all listed in Table I. The inner stray inductance of the MOSFET module is evaluated by the parameters in datasheets provided by the manufacture. It finds that the main stray inductances of the converter are from inner stray inductance of the MOSFETs, the bridge circuit, and the clamping circuit.

TABLE II
SIMULATED PARAMETERS OF CURRENT INVERTER

Parameters	value
Supply voltage of the power	40 V
R_S of the power	2 mOhm
Equivalent inductance of the loop	46 mH
Equivalent resistance of the loop	12 Ohm
Stray capacitance of the loop	5 nF
On-state voltage of MOSFET	2 V
$R_{DS(on)}$ of MOSFET	280 mOhm
C_S of MOSFET	20 pF
R_{D1} and R_{D3}	1000 Ohm

B. Simulations of Current Inverter

Based on the equivalent circuit of the current inverter and its corresponding stray inductance model, the Simulink of the MATLAB software is used to simulate the current of the multi-turn loop.

The simulation is carried out on the conditions that the supply voltage is 40 V and the multi-turn loop is a 1 m×1 m, 128 turns square loop, referring to the ProTEM developed by Geonics of Canada which is one of the most typical and popular TEM system in the worldwide. It has a 1 m×1 m, 128-turn small loop special for the shallow TEM applications. The equivalent inductance of 46 mH and equivalent resistance of 12 Ω are measured at the frequency of 10 kHz by an instrument of impedance analyzer. The equivalent stray capacitance of the loop is then calculated according to the formula (4) of Section II, and the value is set as 5 nF for the simulation. The MOSFET parameters are also considered in the MATLAB Simulink according to the practical parameters of the MOSFET module. The damping resistors R_{D1} and R_{D3} for the simulation are 1000 Ω. All the simulated parameters of the current inverter are listed in Table II.

By using the Zener diode model in the SimPowerSystems library of the MATLAB Simulink, the simulation of the inverter circuit shown in Fig. 7 is completed. The output current and the corresponding output voltage of the inverter is shown in Fig. 8(a). The current pulse rises as an exponential function slowly, and goes to a peak current of 3 A under the power source of 28 V. When the inverter circuit switches off, the current pulse begins to turn-off and the voltage during the turn-off time is a constant clamping voltage of 500 V by the help of the Zener clamping circuit. Obviously, there are big oscillations at the early time of the turn-off current.

Based on the stray inductance model of the current inverter and the lumped parameters of the loop, the detail of the current's turn-off process is shown in Fig. 8(b). It finds that the current does not decay in a perfect linear rule although under the constant clamping voltage of 500 V. According to the characteristics of this turn-off current, it could be divided into three parts: the very early part 1, which decays with serious oscillations, the medium part 2 with high linearity, and the late part 3 with exponential decay. Compared to the ideal current waveform in Fig. 4, this simulated result has serious oscillations in the early part of the falling edge.

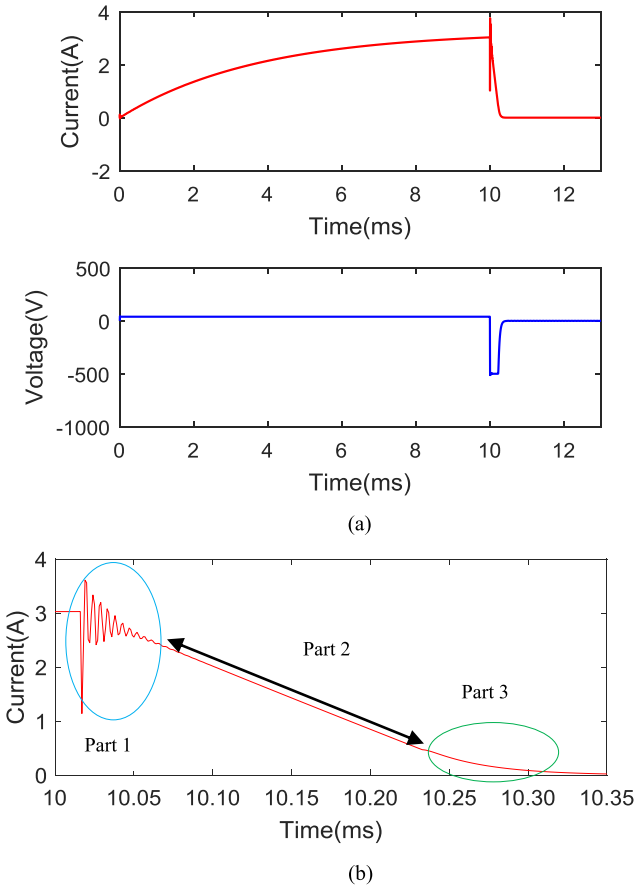

Fig. 8. Simulated results based on the stray inductance model. (a) Simulated current and voltage of the current inverter. (b) Simulated turn-off current in detail.

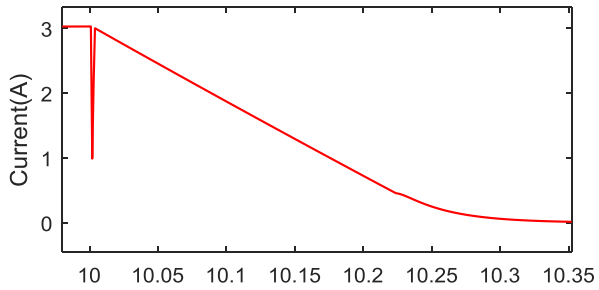

Fig. 9. Simulated turn-off current without considering the stray inductance.

Mostly, the TEM system only considers the loop's parameters and does not include the stray inductance of the current inverter. The corresponding simulated result is shown in Fig. 9. Compared to Fig. 8(b), the serious oscillations do not appear, but only has a reverse pulse with big amplitude at the early part, which is mainly caused by the loop's stray capacitance.

Therefore, the stray inductances of the current inverter circuit and the equivalent lumped parameters of the multi-turn loop are the main reason to cause the high-frequency oscillations at the early part of the turn-off current. In the following part, the experiments are carried out to further analyze and verify the above simulation results.

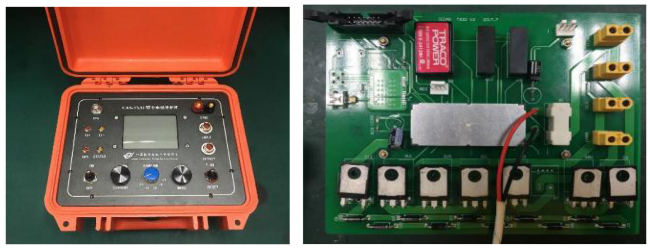

Fig. 10. Prototype of the current inverter and the power PCB board.

TABLE III
PARAMETERS OF CURRENT INVERTER

Parameters	value
Supply voltage	$\leqslant$40 V
Output power	$\leqslant$600 W
Output current	$\leqslant$ 15 A
Pulse repetition frequency	$\leqslant$1 kHz
Turn-off time of current	Linear decay,1us (Minimum)
Synchronization	GPS or Line

Fig. 11. 1 m $\times$ 1 m, 128 turns loop for the current inverter.

IV. EXPERIMENTAL RESULTS AND ANALYSIS

In the experiments, the current inverter, working as a transmitter, is powered by a battery bank of 28 V with good stability. The transmitter prototype shown in Fig. 10 integrates the current inverter with an additional digital control unit and display unit in a small box, so that it is very portable for the shallow TEM survey.

The power devices of the current inverter are chosen according to the maximum voltage and current requirements of inverter circuit design listed in Table III. The isolated diode is DSEI30-10A from IXYS company, the Zener diodes are 1N5369 from ON company with a Zener voltage of 51 V and power of 5 W, and the MOSFET modules of the bridge circuit are SCT2080KE from ROHM company. The power switches of the damping circuit are IRG4BH20K from the IR company. The compact and buck/boost dc/dc power module NQ40W40ETC15NRGS of Synqor company is chosen to provide an adjustable and stable voltage supply from 0 to 40 V.

For the experiment, referring to the ProTEM, we design a same multi-turn loop shown in Fig. 11. The equivalent

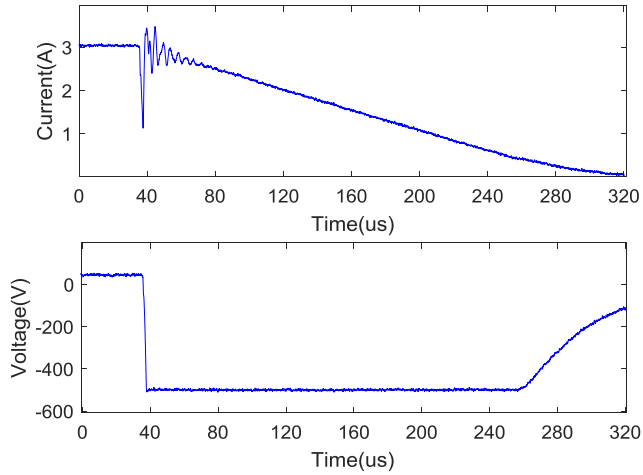

Fig. 12. Measured result of the turn-off current in the loop.

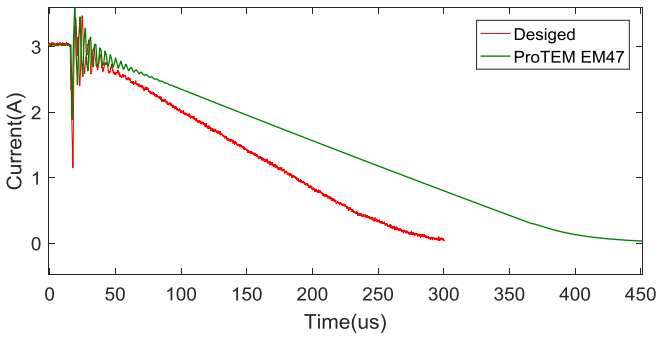

Fig. 13. Comparison of the turn-off current of the current inverter and the EM47.

impedances of the loop are same to the parameters listed in Table II for the above simulations. It is convenient for us to compare and analyze the experimental results and simulated results.

Fig. 12 is the measured results of the 128-turn loop, including measured output current and voltage waveforms. They are measured by the high-accuracy current probe and high-voltage differential probe of Tektronics. The measured amplitude of the current is 3 A, and the constant clamping voltage during the turn-off time is 500 V. The measured turn-off time is 280 μs without current overshoot in the late part. However, the early part of the turn-off current has serious oscillations added to the high linearity falling edge. It means that the high clamping voltage of 500 V could only optimize the linear trend of the turn-off current, and could not suppress or remove the high-frequency current oscillations. The current oscillations of the early part 1 continuous a time of more than 40 us, which will be very bad for the early time electromagnetics responses of the shallow TEM system.

The experiment result is further compared with the commercial TEM system of ProTEM, which has a transmitter EM47 for shallow survey. Under the same condition, the comparison of the measured results of the current inverter and the EM47 is shown in Fig. 13.

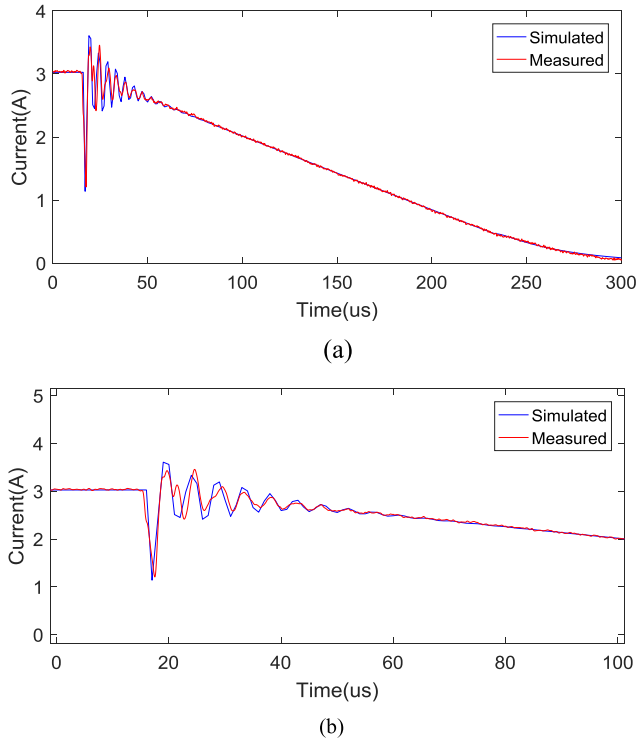

Fig. 14. Measured and simulated turn-off current in the loop. (a) Comparison of the measured and the simulated turn-off current. (b) Comparison of the measured and simulated turn-off current in detail.

It is known that the EM47 also has current oscillations during the turn-off time of 430 μs but smaller than the designed current inverter. The main reason is that the designed inverter has faster turn-off speed under the constant clamping voltage of 500 V, while the EM47 has a longer turn-off time under the constant clamping voltage of 330 V.

The comparison of the measured and simulated turn-off current of the current inverter is shown in Fig. 14(a). The simulated current waveform based on the stray inductance model agrees well with the measured result. Fig. 14(b) is the compared results of early part current oscillations in detail and there is only very small difference between them. The main reason is that the simulated parasitism parameters of the current inverter have small errors. However, it verifies that the established stray inductance model of the current inverter is reasonable and correct to analyze the turn-off current.

Therefore, the stray inductance model of the current inverter in this paper successfully explains the serious high-frequency oscillations of the turn-off current. For the practical TEM applications, the current oscillations in the early time, whatever big or small, will have serious influences on the electromagnetic responses of the shallow TEM surveys. Consequently, it is important to reduce and optimize the stray inductance of the inverter and the stray parameters of the multi-turn loop to suppress the current oscillations.

In this paper, we try to spread the tightly bundled transmitting loop to multi-layer structure to optimize the stray parameters of the loop. The 128-turn loop is divided into 4 layers, and every

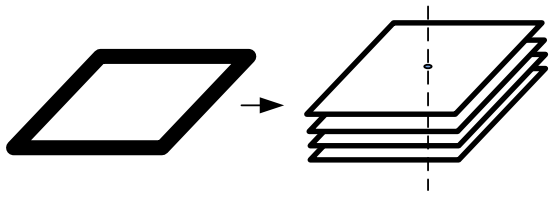

Fig. 15. Multi-layer transmitting loop.

TABLE IV
PARAMETERS OF TWO KINDS OF LOOPS

Parameters	Tightly bundled loop	4 layer loop
Equivalent inductance	46 mH	40 mH
Equivalent resistance	12 Ohm	12 Ohm
Stray capacitance	5 nF	2.1 nF

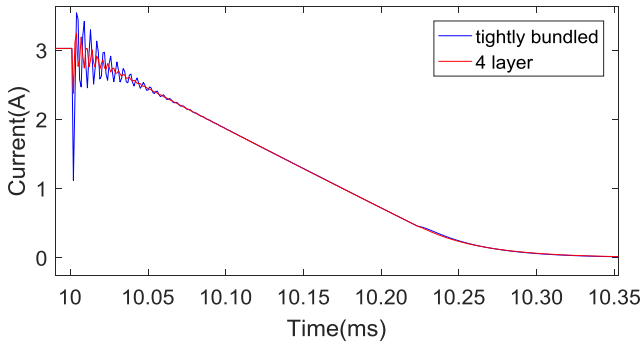

Fig. 16. Turn-off current in the tightly bundled and four-layer loop.

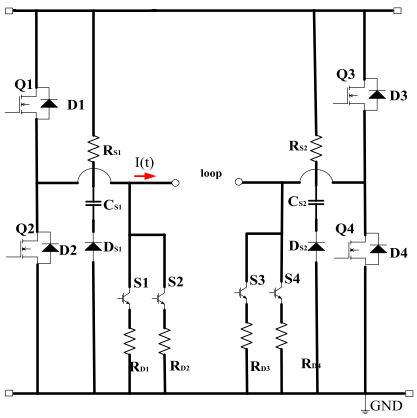

Fig. 17. Snubber circuit for the current converter.

layer has 32 turns. They are parallel and keep a small certain distance vertically shown in Fig. 15. The parameters of the two kind of loops measured at 10 kHz by the impedance analyzer of Agilent are listed in Table IV.

The measured result of tightly bundled and four layer loop is shown in Fig. 16. It finds that the turn-off current of the four layer loop has much smaller oscillations than the tightly bundled loop.

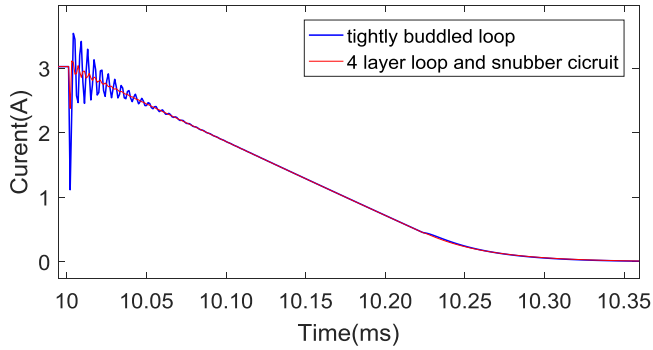

Fig. 18. Turn-off current under the condition of four layers and snubber circuit.

For further suppressing the current oscillations of the inverter, a novel snubber circuit parallel to the IGBTs of the current converter shown as Fig. 17 is proposed. They effectively reduce the influences of the stray inductance of the IGBTs and considerably suppress the electromagnetic interference by optimizing the switching characteristics of the IGBTs.

The measured results of combination of the four layer loop and snubber circuit compared to the tightly buddle loop are shown in Fig. 18. It finds that the current oscillations are further suppressed significantly, thus effectively enhancing the quality of the turn-off current.

V. CONCLUSION

The multi-turn small loop, as a key part to excite the electromagnetic field is widely used for the shallow TEM surveys and other geophysical applications. However, the high-frequency oscillations of the turn-off current do exist in the multi-turn small loop of different applications. Conventionally, the multi-turn loop equals to an *RLC* lumped circuit model, and the stray parameters of the current inverter itself are ignored, thus it fails to explicate the oscillation during the early time of the turn-off current.

In the paper, a novel current inverter with passive clamping for shallow TEM survey is designed and analyzed. The stray inductance model of the current inverter is first established and studied in the TEM system, combined with the *RLC* model of the multi-turn loop, to analyze the turn-off current. Furthermore, the simulation of the turn-off current based on the stray inductance model is finished. At last, the experiments of the current inverter are completed. The simulation results based on the stray inductance model are in good agreement with the measured results. Therefore, the serious oscillations of the turn-off current in the multi-turn loop are perfectly explained and verified by the stray inductance model of the novel current inverter. For suppressing the oscillations of the turn-off current, two suppressing methods, such as multi-layer loop design and novel snubber circuit, are proposed and analyzed. They significantly reduce the current oscillations and thus effectively enhance the quality of electromagnetic response. This will provide new ideas and prospects of early electromagnetic data interpretation for the shallow TEM applications and other geophysics field.

REFERENCES

[1] N. M. Nabighian, *Electromagnetic Methods in Applied Geophysics*, vol. 1. Tulsa, OK, USA: SEG Books, 1988, ch. 4.

[2] S. Wang, C. Yin, J. Lin, Y. Yang, and X. Hu, "Bipolar square-wave current source for transient electromagnetic system based on constant shutdown time," *Rev. Sci. Instrum.*, vol. 87, 2016, Art. no. 034707.

[3] L. Liu, Z. Shi, K. Wu, Z. Geng, and G. Fang, "A bipolar half-sine current inverter for airship-borne electromagnetic (AEM) surveying," *IEEE Trans. Ind. Electron.*, vol. 64, no. 12, pp. 9477–9486, Dec. 2017.

[4] Z. H. Fu, L. W. Zhou, and H. M. Tai, "Current pulse generation for transient electromagnetic applications," *Elect. Power Compon. Syst.*, vol. 35, no. 11, pp. 1201–1218, 2007.

[5] J. A. Ferreira, I. J. Kane, P. Klinkert, and T. B. Hage, "A square-wave current inverter for aircraft-mounted electromagnetic surveying systems," *IEEE Trans. Ind. Appl.*, vol. 40, no. 1, pp. 213–219, Jan./Feb. 2004.

[6] S. Kedarnath and K. Vasudevan, "A novel converter topology for TEM applications," *Sadhana*, vol. 33, no. 5, pp. 537–549, 2008.

[7] D. V. Fitterman and W. L. Anderson, "Effect of transmitter turn-off time on transient soundings," *Geoexploration*, vol. 24, no. 2, pp. 131–146, 1987.

[8] D. H. Bai, "The effect of two types of turn-off current on TEM responses and the correction techniques," *Seismol. Geol.*, vol. 23, no. 2, pp. 245–251, 2001.

[9] Z. H. Fu and L. W. Zhou, "Two novel quasi-resonant step current impulse rectifying circuits," *Proc. CSEE*, vol. 26, no. 5, pp. 70–75, 2006.

[10] M. Kolaj and R. S. Smith, "A multiple transmitter and receiver electromagnetic system for improved target detection," *Geophysics*, vol. 80, no. 4, pp. 247–255, 2010.

[11] R. William, "Step and impulse calculations from pulse-type electromagnetic data," in *Proc. ASEG 15th Geophys. Conf. Exhib.*, Aug. 2001.

[12] R. S. Annan, "Using an induction coil sensor to indirectly measure the B-field response in the bandwidth of the transient electromagnetic method," *Geophysics*, vol. 65, no. 5, pp. 1489–1494, 2000.

[13] N. O. Kozhevnikov, "Damped current oscillations in a horizontal ungrounded loop and their correlation with ground water infiltration," *Doklady Earth Sci.*, vol. 437, no. 2, pp. 544–547, 2011.

[14] C. A. Gallo, F. Tofoli, L. Pinto, and J. A. C. Pinto, "A passive lossless snubber applied to the AC/DC interleaved boost converter," *IEEE Trans. Power Electron.*, vol. 25, no. 3, pp. 775–784, Mar. 2010.

[15] H. G. Zhang, Q. Wang, E. H. Chu, X. C. Liu, and L. M. Hou, "Analysis and implementation of a passive lossless soft-switching snubber for PWM inverters," *IEEE Trans. Power Electron.*, vol. 26, no. 2, pp. 411–426, Feb. 2011.

[16] Q. Li and P. Wolfs, "A current fed two-inductor boost converter with an integrated magnetic structure and passive lossless snubbers for photovoltaic module integrated converter applications," *IEEE Trans. Power Electron.*, vol. 22, no. 1, pp. 309–321, Jan. 2007.

[17] B. K. Sternberg, S. L. Dvorak, and W. Feng, "Design and verification of large-moment transmitter loops for geophysical applications," *J. Appl. Geophys.*, vol. 136, pp. 211–218, 2016.

[18] H. Zhao, L. Liu, K. Wu, Y. Qi, and G. Fang, "Constant voltage-clamping bipolar pulse current source for transient eletromagnetic system," *Electric Power Compon. Syst.*, vol. 41, pp. 960–971, 2013.

[19] H. Luo *et al.*, "Enabling junction temperature estimation via collector-side thermo-sensitive electrical parameters through emitter stray inductance in high-power IGBT modules," *IEEE Trans. Ind. Electron.*, vol. 65, no. 6, pp. 4724–4738, Jun. 2018.

[20] Y. Mukunoki *et al.*, "Modeling of a silicon-carbide MOSFET with focus on internal stray capacitances and inductances, and its verification," in *Proc. IEEE Appl. Power Electron. Conf. Expo.*, 2017, pp. 2671–2677.

[21] T. Suzuki *et al.*, "A built-in high temperature half-bridge power module with low stray inductance and low thermal resistance for in-wheel motor application," in *Proc. Eur. Conf. Silicon Carbide Related Mater.*, 2016, pp. 677–680.

[22] M. Ando and K. Wada, "A normalization procedure of DC-side stray inductance for high-speed switching circuit," in *Proc. IEEE Appl. Power Electron. Conf. Expo.*, 2016, pp. 2986–2991.

[23] L. Yuan *et al.*, "Experimental research on stray inductance extraction of planar bus bars based on HVIGBT dynamic characteristics," in *Proc. 17th Int. Conf. Elect. Mach. Syst.*, 2014, pp. 1957–1962.

[24] C. Chen, X. Pei, Y. Chen, and Y. Kang, "Investigation, evaluation, and optimization of stray inductance in laminated busbar," *IEEE Trans. Power Electron.*, vol. 29, no. 7, pp. 3679–3693, Jul. 2014.

[25] L. Popova *et al.*, "Stray inductance estimation with detailed model of the IGBT module," in *Proc. 15th Eur. Conf. Power Electron. Appl.*, 2013, pp. 1–8.

[26] K. Wada and M. Ando, "Limitation of DC-side stray inductance by considering over voltage and short-circuit current," in *Proc. 15th Eur. Conf. Power Electron. Appl.*, 2013, pp. 1–8.

[27] L. Shengnan, L. M. Tolbert, F. Wang, and F. Z. Peng, "Reduction of stray inductance in power electronic modules using basic switching cells," in *Proc. IEEE Energy Convers. Congr. Expo.*, 2010, pp. 2686–2691.

[28] Z. Wang and G. Chen, "Study on planar busbar regarding stray inductance minimization and oscillation suppression for high power converter," in *Proc. Int. Conf. Sustain. Power Gener. Supply*, 2009, pp. 1–7.

[29] Z. Wang, J. Zhang, X. Wu, and K. Sheng, "Analysis of stray inductance's influence on SiC MOSFET switching performance," in *Proc. IEEE Energy Convers. Congr. Expo.*, 2014, pp. 2838–2843.

[30] L. Müller and J. W. Kimball, "Effects of stray inductance on hard-switched switched capacitor converters," *IEEE Trans. Power Electron.*, vol. 29, no. 12, pp. 6276–6280, Dec. 2014.

[31] O. Muhlfeld and F. W. Fuchs, "Optimization of the stray inductance in three-phase MOSFET power modules aided by means of PEEC simulation," in *Proc. 13th Eur. Conf. Power Electron. Appl.*, 2009, pp. 1–7.

[32] B. Cadilhon, L. Pecastaing, T. Reess, and A. Gibert, "Low-stray inductance structure to improve the rise-time of a Marx generator," *IET Elect. Power Appl.*, vol. 2, no. 4, pp. 248–255, 2008.

[33] G. Engelmann, S. Quabeck, J. Gottschlich, and R. W. De Doncker, "Experimental and simulative investigations on stray capacitances and stray inductances of power modules," in *Proc. 19th Eur. Conf. Power Electron. Appl.*, 2017, pp. 1–10.

Lihua Liu received the M.S. degree in electrical engineering from the HuaZhong University of Science and Technology, Wuhan, China, in 2007, and the Ph.D. degree from the Chinese Academy of Sciences (CAS), Beijing, China, in 2010.

Since 2010, she has been with the Key Laboratory of Electromagnetic Radiation and Sensing Technology, Institute of Electronics, CAS, where she has been an Associate professor. Her main research interests include geophysical detection and system design, power electronics technology and application in the electromagnetic detection, pulse technology of microwave propagation, and remote sensing radar.

Liu Qiao received the B.S. degree in electronic information engineering from Yunnan University, KunMing, China, in 2016. He is currently working toward the master's degree in integrated circuit engineering at the Institute of Electronics, Chinese Academy of Sciences (CAS) and University of Chinese Academy of Sciences, Beijing, China.

His research interests include design of transient electromagnetic system in geophysics and power source technology.

Leisong Liu received the M.S. degree from the Institute of Electronics, Chinese Academy of Sciences, Beijing, China, in 2010.

He is currently a Research Associate with the Institute of Electronics, Chinese Academy of Sciences.

His main research interests include high sensitivity magnetometer and low noise amplification technology.

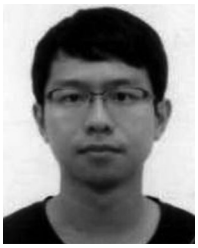

Zhi Geng received the B.S. and M.S. degrees in automation and electrical engineering from Northeastern University, Shenyang, China, in 2010 and 2012, respectively.

Since 2012, he has been a Lecturer with the Institute of Electronics, Chinese Academy of Sciences, Beijing, China. His research interests include power electronics technology application in the electromagnetic detection, power source technology, dc–dc converters, and modeling and control of switching power supplies.

Zongyang Shi received the B.S. degree in electronic information engineering from the University of Science and Technology of China (USTC), Hefei, China, in 2013. He is currently working toward the Ph.D. degree in electromagnetic field and microwave at the Institute of Electronics, Chinese Academy of Sciences (CAS) and University of Chinese Academy of Sciences, Beijing, China.

His research interests include design of transient electromagnetic system in geophysics, EM signal processing technology, and remote sensing applications.

Guangyou Fang received the B.S. degree in electrical engineering from Hunan University, Changsha, China, in 1984, and the M.S. and Ph.D. degrees in electrical engineering from Xi'an Jiaotong University, Xi'an, China, in 1990 and 1996, respectively.

From 1990 to 1999, he was an Engineer, Associate Professor, and a Professor with the China Research Institute of Radiowave Propagation. From 2000 to 2001, he was a Visiting Scholar with the University of Trieste, Trieste, Italy, and with the International Center for Science and High Technology, United Nations Industrial Development Organization, Trieste. From 2001 to 2003, he was a Special Research Fellow of the Japan Society for the Promotion of Science, working with Prof. M. Sato, with Tohoku University, Sendai, Japan. Since 2004, he has been a Professor with the Institute of Electronics, Chinese Academy of Sciences, Beijing, China, where he is the Director of the Key Laboratory of Electromagnetic Radiation and Sensing Technology. He has authored more than 100 publications. His research interests include ultra-wide band radar, ground penetrating radar signal processing and identification methods, terahertz imaging technology, and computational electromagnetic.